ACS OMEGA

Open Access

http://pubs.acs.org/journal/acsodf

Article

Photoassisted Water Purification through an Electrochemically Artificially Adjusted p-Cu_2O Light Absorption Layer

Dhruv Sharma,[‖] Dong Su Kim,[‖] Shin Young Oh, Kun Woong Lee, Won Seok Yang, Xuan Zhang, Sanjay Kumar Swami, Hyung Koun Cho,* and Sung Woon Cho*

Cite This: *ACS Omega* 2024, 9, 29723−29731

Read Online

ACCESS | Metrics & More | Article Recommendations | Supporting Information

ABSTRACT: The implementation of photoelectrochemical water purification technology can address prevailing environmental challenges that impede the advancement and prosperity of human society. In this study, Cu, which is abundant on Earth, was fabricated using an electrochemical deposition process, in which the preferential orientation direction and carrier concentration of the Cu-based oxide semiconductor were artificially adjusted by carefully controlling the OH^- and applied voltage. In particular, Cu_2O grown with a sufficient supply of OH^- ions exhibited the (111) preferred orientation, and the (200) surface facet was exposed, independently achieving 90% decomposition efficiency in a methyl orange (MO) solution for 100 min. This specialized method minimizes the recombination loss of electron−hole pairs by increasing the charge separation and transport efficiency of the bulk and surface of the Cu_2O multifunctional absorption layer. These discoveries and comprehension not only offer valuable perspectives on mitigating self-photocorrosion in Cu_2O absorbing layers but also provide a convenient and expeditious method for the mass production of water purification systems that harness unlimited solar energy. These properties enable significant energy saving and promote high-speed independent removal of organic pollutants (i.e., MO reduction) during the water purification process.

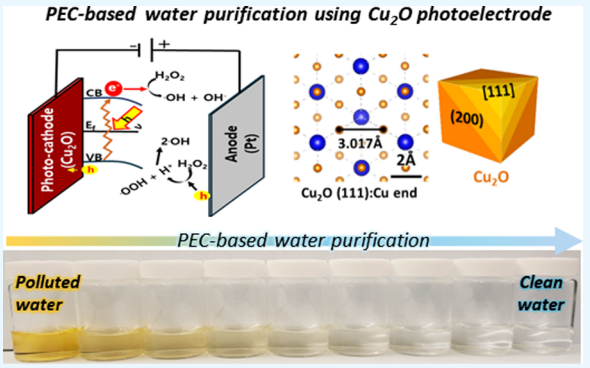

1. INTRODUCTION

The world faces significant environmental issues, such as water pollution,[1−3] due to rapid urbanization and industrialization. A diverse range of refractory organic pollutants present in wastewater and surface water, including persistent organic pollutants (POPs), pharmaceutical and personal care products (PPCPs), and endocrine disruptors,[4−6] pose direct or indirect risks to human health because of their considerable stability and toxicity.[7,8] Hence, employing proficient techniques to eradicate these contaminants from aquatic ecosystems is important.[9−11] To achieve this, various techniques, including flocculation, adsorption, filtering, and biodegradation, are employed.[12]

Solar energy, an inexhaustible and environmentally friendly energy source, holds immense potential as a sustainable solution for meeting global energy demands.[13] Ongoing research explores diverse solar energy technologies and uses that may effectively harness this vast resource.[13−15] Photoelectrochemistry-based water purification is a promising method for generating clean water because of its favorable environmental impact, cost-effectiveness, and potential for large-scale implementation.[16−19] The fundamental aspects of solar energy assistance are energy conservation and a rapid response time. Moreover, implementing photoelectrodes incorporating an extra layer for light absorption facilitates convenient recycling and removal. In a scenario involving a light-absorbing layer with the ability to absorb visible light, solar irradiation can result in the absorption of light energy, forming electron−hole pairs (EHPs). It is crucial to understand the reduction in recombination loss in EHPs generated within the semiconductor absorption layer. This understanding should be effectively used to facilitate prompt charge separation and required chemical reactions.[20−22]

Several semiconductors can effectively capture solar energy, such as CIS (with a band gap energy of 1.9 eV), SnS, Se_2Sb_3, TiO_2 (3.0 eV), WO_3 (2.8 eV), $BiVO_4$ (2.4 eV), Fe_2O_3 (2.3 eV), and Cu_2O (2.1 eV).[15,16,20−2122] Thus, cuprous oxide (Cu_2O) is a viable candidate for developing photocathodes in the field of photoelectrochemical (PEC) water purification.[23−27] This is primarily attributed to its favorable band gap (2.1 eV), which enables efficient light absorption. In addition, Cu_2O possesses other desirable characteristics, including a straightforward electrochemical growth process,

Received: April 4, 2024
Revised: June 4, 2024
Accepted: June 21, 2024
Published: June 28, 2024

the ability to be manufactured on a large scale, nontoxic properties, controlled aspects, and widespread availability of resources.[28−30] The primary observation is that the electrochemical growth direction of Cu_2O aligns well with the direction of electron movement in the context of PEC water filtration. Furthermore, the Cu_2O photocathode can produce a photocurrent of up to 14.7 mA·cm^{-2} via PEC water splitting.[31] Nevertheless, in the context of PEC water splitting, the Cu_2O photocathode exhibits a preference for photocorrosion over water decomposition. This preference arises from the self-redox state within the band gap, which makes the photocorrosion reaction kinetically more favorable. To mitigate this issue, four functional layers, namely, absorption and buffer layers, were employed to suppress undesired photocorrosion reactions.[32−34] To achieve the desired outcome, investigating and developing several components, including the catalyst, protective layer, and cocatalyst, is necessary. This undertaking presents numerous technological challenges owing to the need for comprehensive material exploration and collaboration. Hence, the p-Cu_2O layer primarily serves as an absorption layer in water splitting applications. However, in the context of PEC water purification, it ensures stability and acts as a catalyst for water purification in conjunction with its absorption capabilities.[35−38]

In this study, we propose a novel electrochemical growth approach for controlling nucleation during the development of Cu_2O to produce a thin film with a crystal structure that facilitates electron movement for PEC water purification. In addition, this approach formed a high-density surface. This development represents the progress in the respective fields. The nucleation of Cu_2O was influenced by the variations in the pH and growth voltage of the electrochemical solutions. The subsequent grain orientation may be precisely regulated by initially promoting dense nucleation. Furthermore, the charge separation process was enhanced by manipulating the Fermi level of Cu_2O to generate significant band bending.

The charge recombination loss was effectively mitigated by reducing the internal resistance of the Cu_2O light absorption layer. This was achieved by electrochemically controlling the nucleation process, resulting in a dense and uniform surface morphology of Cu_2O. Consequently, the electrolyte performance was enhanced, reducing the charge recombination loss by up to 50%. At this time, Cu_2O has a maximum photocurrent of 3.5 mA·cm^{-2} at 0 V_{RHE}. Notably, no significant decrease in the photocurrent over time was detected, indicating sustained performance. Moreover, the long-term stability of Cu_2O was confirmed. These findings not only provide insight into suppressing the self-photocorrosion of Cu_2O light-absorbing layers but also provide an easy and fast approach for large-scale fabrication for water purification using infinite solar energy.

2. EXPERIMENTAL SECTION

2.1. Chemicals and Materials. $CuSO_4$ (copper sulfate) and $C_3H_6O_3$ (latic acid solution, 85% aqueous solution) purchased from Merck were used without further purification. NaOH (sodium hydroxide), H_2O_2 (hydrogen peroxide, 35 wt % solution in water), and methyl orange (MO) solution (0.1%, indicator pH 3.1−4.4) were used without purification and purchased from Fluka.

2.2. Synthesis of Cu_2O Electrodes. Cu_2O films were deposited electrochemically on indium tin oxide (ITO)-coated glass substrates measuring 15 mm × 40 mm and having a resistance of 15−20 Ω/sq. Before the deposition, the substrates were cleaned using acetone and 2-isopropyl alcohol and deionized water for 15 min each in an ultrasonicator. The cleaned substrates were then subjected to ultraviolet (UV) treatment for 20 min. The electrolyte solution for Cu_2O deposition was prepared by mixing 0.4 M anhydrous copper sulfate with a 3 M lactic acid solution and adjusting the pH using 4 M sodium hydroxide. The Cu_2O films were deposited using a potential of −0.3, − 0.5, and −0.7 V vs Ag/AgCl ($V_{Ag/AgCl}$), respectively, with a Pt mesh counter electrode at 60 °C.

2.3. Material Characterization. Using X-ray diffraction (XRD, Bruker AXS D8 Discover, Cu Kα radiation source), field-emission scanning electron microscopy (FE-SEM; JSM-6700F, JEOL, 10 kV) with an accelerating voltage of 200 keV was used for image observation. The optical characteristics of the photocathodes were investigated using a UV−Vis-NIR spectrometer (Cary5000, Agilent) with an integrating sphere ranging from 400 to 800 nm.

2.4. Photoelectrochemical Water Purification Analysis. A three-electrode system with a Versastat 3 potentiostat was used for photoelectrochemical purification of an electrolyte solution containing MO under illumination. A 150 W xenon lamp calibrated with an AM 1.5G filter was used as the light source for 1 sunlight illumination, with a light intensity of 100 mW·cm^{-2}, measured using a standard silicon photodetector. H_2O_2 was added to the electrolyte solution containing MO. This increases the generation of hydroxyl radicals ($^{\bullet}OH$) and promotes the decomposition of MO, thereby enhancing water purification efficiency. Chronoamperometric (CA) measurements were conducted to evaluate the performance of the Cu_2O-based water purification system. Samples of the decolorized water were collected at regular intervals and analyzed using a UV−Vis-NIR spectrometer to monitor the degree of purification. Linear sweep voltammetry (LSV) and cyclic voltammetry (CV) scans were performed along the positive direction with a scan rate of 10 mV·s^{-1} in the dark and illuminated states. The water containing MO was purified for 15, 30, 45, 60, 75, 90, 105, and 120 min, and the nonpurified solution was dyed with 250 μL of MO, which corresponds to the average polluted water, to evaluate the photodegradation performance. Electrochemical impedance spectroscopy (EIS) was measured from 10^{-3} to 10^{6} Hz with an amplitude of 10 mV and recorded at a bias of 0 V_{RHE} in the dark and illuminated states. Mott−Schottky plots were obtained from 0 to 0.7 V_{RHE} with a frequency of 10^{3} Hz. During the investigation of PEC performance, all potentials (versus Ag/AgCl) were converted to the RHE condition using the Nernst eq 1

$$E_{RHE} = E_{Ag/AgCl} + 0.1976 + (0.0591 \times pH) \text{ at } 25\ ^{\circ}C \quad (1)$$

In the Mott−Schottky measurements, the photoanode donor density (N_D) was calculated as follows, using eq 2

$$N_D = \frac{2}{\varepsilon\varepsilon_0 e}\left(\frac{d(1/c)^2}{dV}\right)^{-1} \quad (2)$$

where ε is the relative permittivity (5.1160 for Cu_2O), ε_0 is the vacuum permittivity (8.85 × 10^{-12} F·m^{-1}), and e is the electronic charge (1.602 × 10^{-19} C).

https://doi.org/10.1021/acsomega.4c03234
ACS Omega 2024, 9, 29723−29731

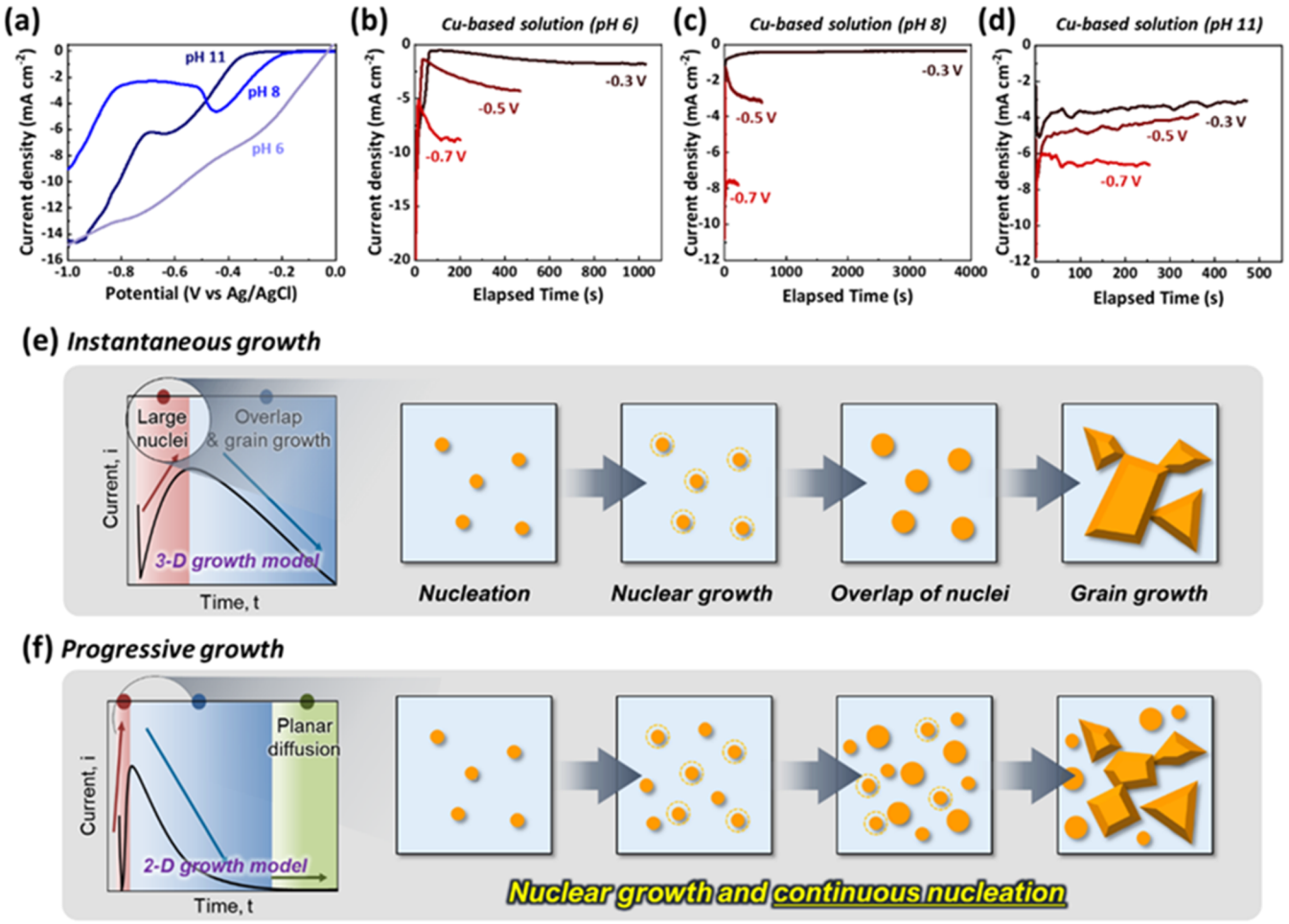

Figure 1. (a) Linear sweep voltammetry (LSV) data of Cu-based solution showing the various pH concentrations. (b–d) Chronoamperometry (CA) data during electrochemical deposition of Cu-based materials. (e, f) Diagram of Cu_2O nucleation and growth.

3. RESULTS AND DISCUSSION

The suggested sequence of chemical reactions for the growth of Cu_2O thin films on conductive substrates by electrochemical deposition involves successive occurrence of the following steps starting with a Cu (II) salt solution.

$$2Cu^{2+} + 4L^{-} \rightarrow 2(Cu_{II}\text{-}L_2)\ (L^{-}:\ \text{lactate ion}) \quad (3)$$

$$2(Cu_{II}\text{-}L_2) + 2e^{-} \rightarrow 2Cu^{+} + 4L^{-} \quad (4)$$

$$2Cu^{+} + 2OH^{-} \rightarrow 2(Cu_{I}OH) \quad (5)$$

$$2(Cu_{I}OH) \rightarrow Cu_2O + H_2O \quad (6)$$

Based on the Pourbaix diagram (Figure S1), Cu^{2+} ions reacted with OH^{-} ions in aqueous solution in the absence of an applied potential, reducing Cu^{2+} to the $Cu(OH)_2$ phase. Nevertheless, upon dissolution of the lactate ions in the solution, a copper-lactate (Cu_{II}-L_2) phase forms, as described in reaction 3. Subsequently, this phase is reduced to Cu^{+} at the surface of the electrode following the reduction potential outlined in reaction 4. The OH^{-} ions present in the electrolytes promptly bind to the unpaired bonding sites of the Cu^{+} ions, forming $Cu_{I}OH$ as an intermediate phase, as indicated by reaction 5. The Cu_2O phase was formed as a result of the dehydration and condensation of $Cu_{I}OH$, as described in reaction 6.

Figure 1a illustrates the standard LSV profiles acquired at 60 °C in electrolyte solutions, including 0.3 M $CuSO_4$ and 4 M lactate, with pH levels ranging from 6 to 11. The observed geometries of these curves are in accordance with those previously reported for analogous electrolytes. As shown in Figure 1a, at pH 6, no significant inflection points are observed in the LSV curve. However, noticeable variations among the three distinct sections were evident at pH 8 and 11. This observation aligns with the Pourbaix diagram of Cu-based oxides, as shown in Figure S1. At pH 6, Cu metal (Cu^0) formation was favored when the voltage was negative. At pH 8 and 11, homogeneous Cu_2O (Cu^{II}) and heterogeneous Cu-based phase [Cu_2O (Cu^{II}) + Cu (Cu^0)] can be formed. These reactions can be categorized into three distinct stages, each resulting in Cu (Cu^0) reduction. To produce a thin layer of Cu_2O oxide semiconductor with light absorption capabilities, electrodeposition was conducted using three different electrolytes at specific voltages of −0.3, − 0.5, and −0.7 $V_{Ag/AgCl}$. The electrolytes were separated into three portions, each at pH 11. Here, the same charge amount (1.5 C) was injected. The CA results shown in Figure 1b–d provide a comprehensive illustration of the changes in current that occur during the electrodeposition procedure for each electrolyte, offering a detailed analysis. The electrochemical growth evolution of thin films can be categorized into four stages: nucleation, nuclear growth, nuclear overlap, and grain growth. The process can be

https://doi.org/10.1021/acsomega.4c03234
ACS Omega 2024, 9, 29723−29731

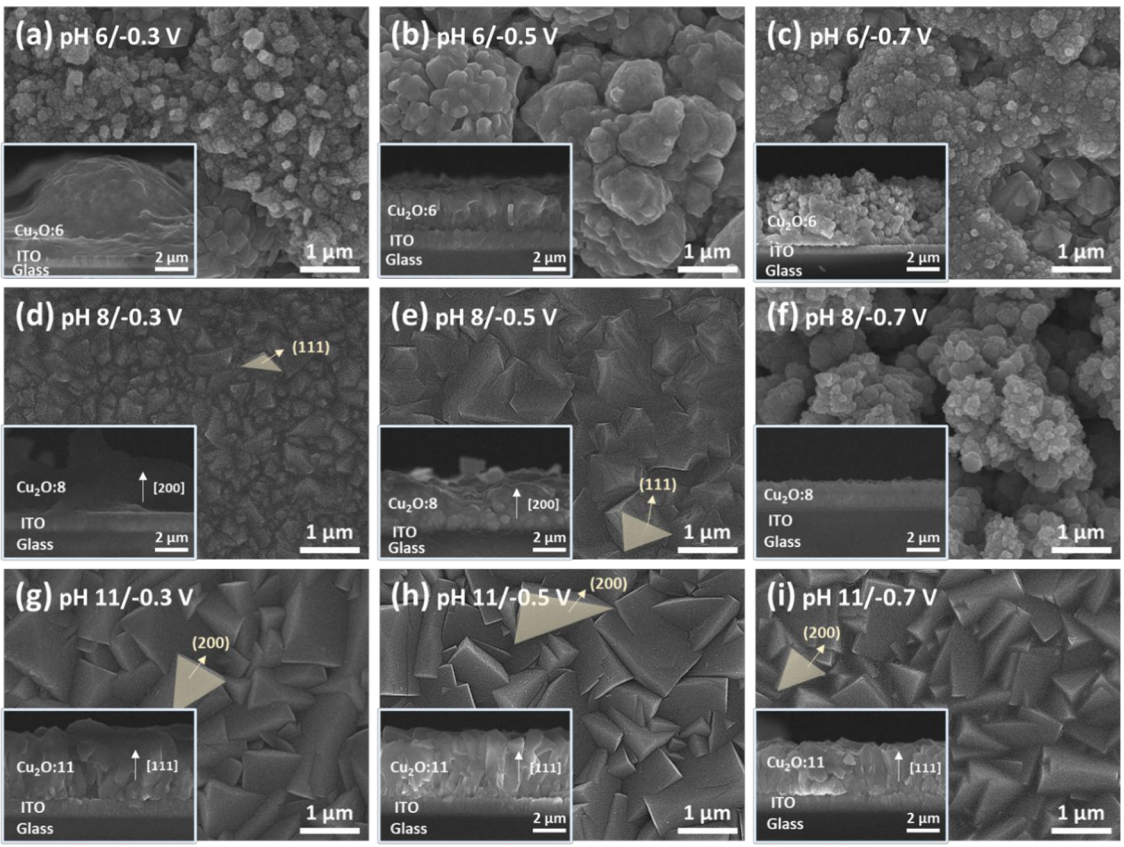

Figure 2. Plan and cross-view SEM images of Cu_2O products. (a−c) Cu partials at pH 6, (d−f) quadrangular pyramid at pH 8 triangular, and (g−i) perfect triangular pyramid at pH 11.

classified into two different types: instantaneous growth, where nucleation and growth occur separately, and progressive growth, where nucleation and growth occur simultaneously (see Figure 1e,f). At a pH of 6, when subjected to applied voltages of −0.3, − 0.5, and −0.7 $V_{Ag/AgCl}$, the nucleation time (t_{max}) was 3.01, 1.14, and 0.31 s, respectively. In addition, the density of the Cu nuclei increased with higher applied voltages, leading to a shift toward dense progressive development. In the electrolyte with a pH of 8, the t_{max} drops to 1.27, 0.91, and 0.56 s when the voltage increases. This finding supports the notion of a proportionate association between nucleation and applied voltage. Under alkaline conditions at pH 11, the synthesis of Cu_2O is accelerated. The t_{max} values for the formation of Cu_2O are observed at −0.3 and −0.5 $V_{Ag/AgCl}$, with corresponding values of 6.91 and 1.61 s, respectively. In contrast to the faster formation of Cu metal at pH 6 and 8, the formation process was slower across different pH settings. However, at pH 11, when an applied voltage of −0.7 $V_{Ag/AgCl}$ is employed, the formation process demonstrates a rapid rise, reaching a value of 0.27 s. This observation is illustrated in Figures 1a and S1. The combination of Cu_2O (Cu^{II}) and Cu (Cu^0) was prepared, creating a favorable environment for potential development.

Further insight into the mechanism of electrochemical deposition was obtained by comparing the Cu-based films prepared using the three electrolytes, as shown in Figure 2. Figure 2a−c shows the dispersion of Cu^0 particles at a low concentration of pH. In this experimental setup, when just an applied voltage of −0.3 $V_{Ag/AgCl}$ is used (as shown in Figure 2a), the nuclear density reaches its minimum value. In addition, the film shows high surface roughness, which may be attributed to the instantaneous development process, compatible with the behavior shown in Figure 1b. The thin films grown with a pH of 8 exhibit significant cubic characteristics when subjected to applied voltages of −0.3 and −0.5 $V_{Ag/AgCl}$. Furthermore, as a result of limited OH^- availability, the crystal grew along the [200] orientation, resulting in a pyramidal morphology characterized by the exposure of the (111) surface facet. In comparison, the thin film grown under a pH of 11 exhibited growth mostly in the [111] orientation, which may be attributed to the abundant availability of OH^- ions. This growth resulted in the exposure of the (200) surface facets, as shown in Figure 2g−i. Figure S2 shows optical images of the thin films corresponding to each electrolyte and voltage. In a unit cell of copper(I) oxide (Cu_2O) with a cubic crystal structure, the oxygen atoms are positioned tetragonally inside the face-centered cubic (FCC) copper framework. The Cu (111) surface is characterized by the presence of oxygen ions, which form ionic bonds with copper in 1:1 and 3:1 ratio. Particularly, Cu−O ionic bonding occurred with 25 and 75% distributions, respectively. By contrast, the (200) surface plane exhibited a well-organized arrangement of copper (Cu) ions and oxygen (O) ions, whereby two Cu ions were bonded with one O ion. Therefore, considering the spatial variation in the density of oxygen atoms per unit area on the Cu^+-terminated surfaces is important.

Figure 3a,b shows top-view images illustrating the spatial configurations of Cu^+ ions on the Cu_2O (200) and (111) planes, respectively. These arrangements are particularly interesting since they are involved in the subsequent reaction with O^{2-} ions. Theoretically, the density of oxygen atoms per

https://doi.org/10.1021/acsomega.4c03234
ACS Omega 2024, 9, 29723−29731

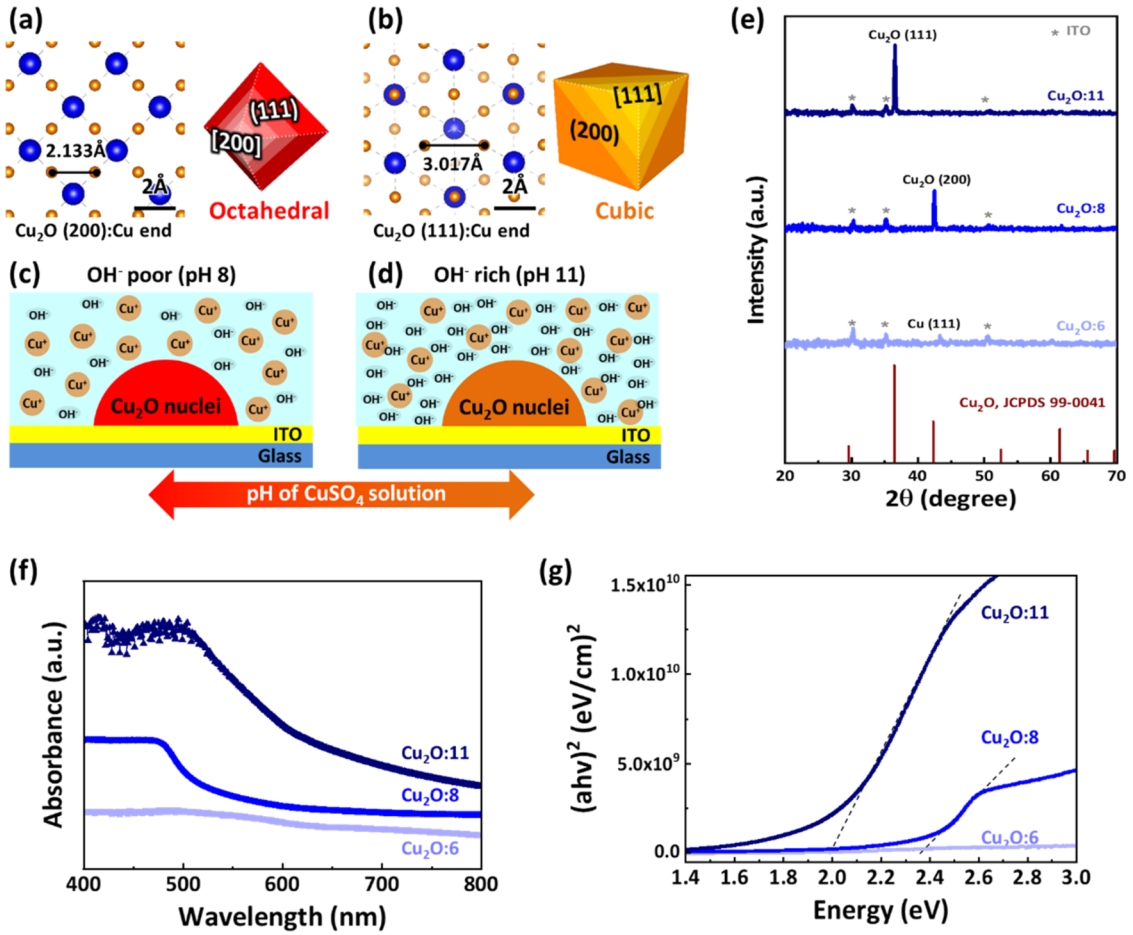

Figure 3. On (a) the (200) and (b) the (111) surfaces, various amounts of Cu-end are present. Schematics of nucleation at pH 8 (c) and pH 11 (d). XRD data of (e) Cu_2O films prepared with different OH^- ion concentrations. (f) UV−Vis−NIR absorption spectra with different OH^- ion concentrations. (g) Tauc plots of Cu_2O:6, Cu_2O:8, and Cu_2O:11 thin films.

unit area on the copper surfaces is estimated to be around 7.31 and 3.88 atoms·nm^{-2} on the (111) and (200) planes, respectively. The provision of oxygen atoms in the solution is facilitated by the presence of OH^- ions. However, the use of weakly basic electrolytes with a pH range of 8−9 results in an inadequate supply of OH^- ions. Consequently, the overall growth behavior is ultimately dictated by the mass transit of OH^- ions to the surface of the electrode (Figure 3c). Consequently, the (200) plane, which has a lower demand for oxygen ions, is favorable for crystal growth. This preference led to the development of Cu_2O crystal phases with a predominant [200] orientation. This phenomenon was supported by the formation of pyramid-shaped crystals with (111) surface facets and a quadrangular base, as shown in Figure 2e. By contrast, when the solution was moved to a strong base with a pH of approximately 11 (Figure 3d), the growth behavior was no longer affected by the concentration of OH^- ions. Instead, it is primarily determined by the surface bonding efficiency associated with the surface energy. From a crystallographic standpoint, it can be observed that the (111) Cu_2O surface exhibits a preference for growth owing to its ability to minimize surface energy. This preference is attributed to the presence of a significant number of Cu^+ dangling bonds on the surface. Consequently, the exposure of the (200) sidewalls under high-pH conditions led to the formation of pyramid-shaped crystals with a triangular base (Figure 2h,i). The preferential growth direction of Cu_2O was closely related to the bulk and surface electrical conductivities of the thin films. The (111) facets are highly conductive, whereas the (100) facets are only moderately conductive. The {110} facets were nonelectrically conductive. Additionally, the optimal way to reduce recombination loss is to form a grain that matches the direction of electron−hole movement in a circuit for electrochemical and photoelectrochemical reactions. Cu_2O formation is an important step in the electrodeposition method because the bath pH, concentration, temperature, applied potential, and deposition time are maintained simultaneously. We fixed the applied voltage at −0.5 $V_{Ag/AgCl}$ and observed the XRD pattern according to the change in OH concentration in Figure 3e. The thin films grown at pH 6, 8, and 11, respectively, are named Cu_2O:6, Cu_2O:8, and Cu_2O:11. For the Cu_2O thin films, the peaks at 36.6 and 42.5° were attributed to the (111) and (200) planes, respectively (JCPDS file number 99-0041). Cu_2O:6 was formed, with Cu as the dominant metal. The Cu_2O:8 thin films exhibit the (200) plane as the preferential growth direction. As expected, Cu_2O:11 grown in an environment with sufficient OH^- ion supply grew strongly preferentially in the [111] direction, exposing the (200) surface facet. This indicates that it has an excellent crystal structure. In addition, the appearance of hkl planes with different maximum intensities in the Cu_2O thin films was due to the increased supply of OH^- ions at a constant bath temperature. The corresponding absorption

https://doi.org/10.1021/acsomega.4c03234
ACS Omega 2024, 9, 29723−29731

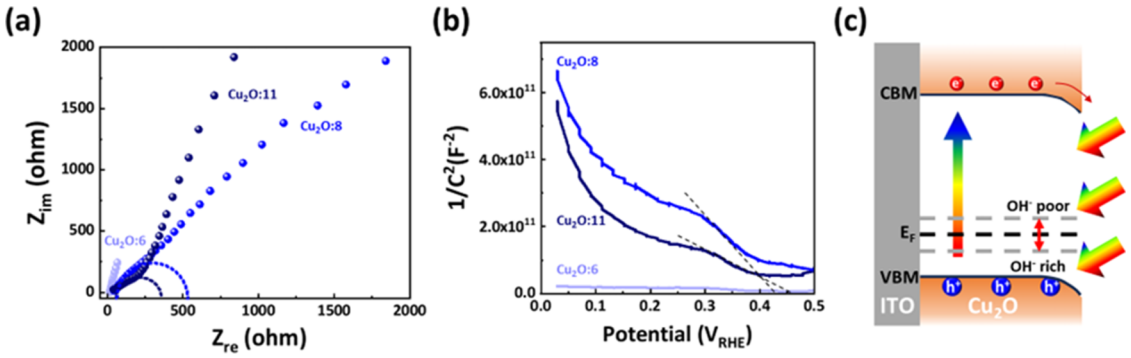

Figure 4. (a) Results of electrochemical impedance spectroscopy (EIS) performed under AM 1.5G illumination on Cu_2O:6, Cu_2O:8, and Cu_2O:11 electrodes, respectively. (b) Mott−Schottky plots for Cu_2O:6, Cu_2O:8, and Cu_2O:11 in 1 M Na_2SO_4 electrolyte buffered with H_2SO_4 in the dark. (c) Band diagram of each Cu-based thin film according to the change in concentration of OH^- ions supplied during the electrodeposition process.

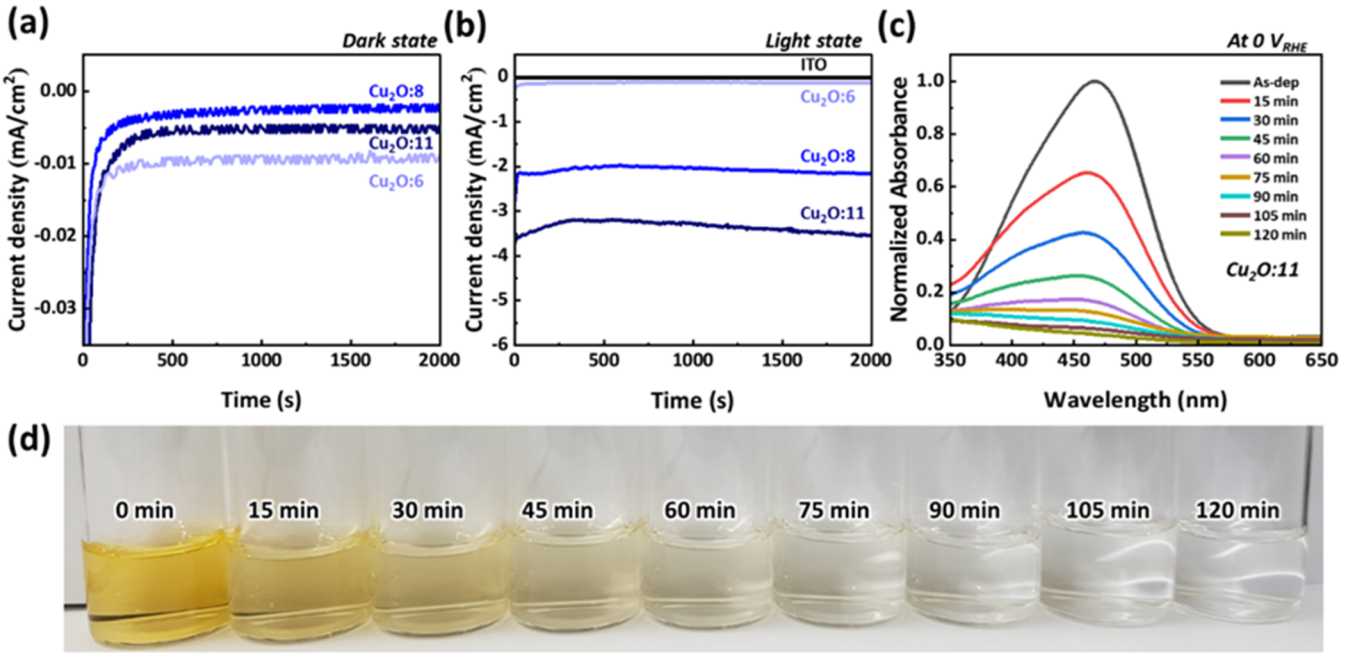

Figure 5. (a, b) Long-term stability test of photoelectrodes at 0 V_{RHE} in 1 M Na_2SO_4, 0.5 M H_2O_2, and 0.5 M methyl orange solution under dark or AM 1.5G illumination. (c) UV−Vis absorption spectra of MO; (d) colors of solutions.

spectra (Figure 3f) exhibited a similar band edge to that of Cu_2O. The associated band gap was calculated using eq 7

$$\alpha h\nu = A(h\nu - E_g)^{\eta} \tag{7}$$

where α, h, ν, E_g, and A are the absorption coefficient, Planck's constant, light frequency, band gap energy, and a proportionality constant, respectively. The variable η depends on the nature of the optical transition during photon absorption. For direct band gap materials such as Cu_2O, E_g can be estimated from a Tauc plot of $(\alpha h\nu)$ versus $h\nu$, wherein $\eta = 0.5$, with the optical absorption coefficient obtained from the Kubelka−Munk function, giving E_g of 2.00 and 2.35 eV, respectively, for pH 11 and pH 8 Cu_2O thin films (Figure 3f,g). As confirmed by XRD, Cu_2O:6 was mainly composed of Cu metal; therefore, it hardly absorbed visible light. Thin films formed in each of the preferential growth directions of [111] and [200] can absorb sunlight sufficiently. Cu_2O:11, which has a narrower band gap, is a potential candidate for an excellent sunlight absorption layer.

To obtain a comprehensive understanding of the charge transport occurring in the bulk and the charge transfer occurring at the surface across the interface of the photocathode and electrolyte, EIS was performed. This study was conducted on several samples, and the measurements were performed under dark conditions. Analysis of the EIS findings relies on the use of an appropriate resistance-capacitance (RC) model, which serves to discern the significant temporal scales associated with charge transfer during investigations involving PEC water purification. Nyquist plots for the unaltered and modified Cu_2O or Cu photocathodes and the corresponding RC circuits were used to analyze the EIS findings. In the RC model, R_s represents the presence of a series of resistances between the ITO and Cu-based thin-film layers. In Figure 4a, the thin film formed at pH 6 has the smallest R_s of 16 Ω owing to its metallic properties. The thin films formed at pH 8 and 11 are 42 and 40 Ω, respectively. The resistance R_{trap} reflects the phenomenon of charge accumulation and trapping inside the Cu-based thin-film layers. The phenomenon known as $R_{ct,ss}$ represents the resistance encountered during charge transfer between the surface states of the photocathode and the

https://doi.org/10.1021/acsomega.4c03234
ACS Omega 2024, 9, 29723−29731

electrolyte. The capacitances C_{bulk} and C_{ss} correspond to the space-charge capacitances of the bulk and surface states of Cu_2O (Cu^0) in the electrolyte, respectively. The required resistances and capacitances were generated from the best fit obtained by fitting the EIS data to the RC model. pH 6 Cu-based film with metal properties does not form semicircles; by contrast, Cu_2O:8 and Cu_2O:11 with semiconductor properties form semicircles. Here, R_{trap} can be converted to the diameter of the semicircle and is related to the series resistance within the bulk of the material. Cu_2O at pH 8 exhibits a R_{trap} of 510 Ω, but Cu_2O:11, which has undergone strong preferential growth with [111], has 275 Ω and a relatively low bulk resistance, making it advantageous for transporting the formed electron−hole pair without recombination loss. Mott−Schottky analysis was used to determine the donor density and flat-band potential (E_{FB}) at the interface between the semiconductor and liquid. In addition, the Mott−Schottky plot was analyzed at 1000 Hz for the Cu_2O surface. The three photocathodes showed negative slopes (Figure 4b), indicating p-type semiconductor properties. The sample with Cu_2O:11 exhibited a smaller slope in the Mott−Schottky plot than Cu_2O:8, which suggests an increase in the donor density. The flat-band potentials of Cu_2O:8 and Cu_2O:11, calculated from the *x-intercepts* of the linear region, are 0.45 and 0.5 V_{RHE}, respectively. The Cu_2O photocathode preferentially grown in the [111] direction exhibited an increased flat-band potential of 50 mV, which can also increase the photovoltage. This change suggests that the Fermi level can be easily controlled by carefully controlling the electrochemical process during Cu_2O thin-film growth, as shown in Figure 4c. Furthermore, the band bending between the light absorption layer and the electrolyte can be tuned.

To demonstrate the impact of the preferred orientation of Cu_2O on the separation and transport of photogenerated charge carriers, photocurrent measurements at 0 V_{RHE} were performed by depositing these materials on ITO electrodes (Figure 5a,b). As shown in Figure 5a, the CA of each thin film was measured at an applied voltage of 0 V in the dark. Cu_2O:6, which has metallic properties, exhibited the highest current density. However, in the CA shown in Figure 5b, where sunlight is irradiated, Cu_2O:6 barely absorbed visible light and exhibited a current density of ∼0.2 $mA{\cdot}cm^{-2}$. Unlike the other cases, Cu_2O:11 shows the highest photocurrent density of ∼3.5 $mA{\cdot}cm^{-2}$. This means that the electrons and holes generated in Cu_2O:11 can be separated and transferred more effectively, compared to other cases. MO is a typical color contaminant in wastewater. The purpose of PEC degradation of organic dyes is to decompose them into small, nonpolluting organic molecules, such as organic acids and CO_2. Cu-based oxide photocathodes have been well known for decades for their catalytic activities. Cu_2O contains active tetrahedral sites on its surface facet, making it suitable for photoabsorption and photocatalysis. Considering this, we performed dye degradation experiments using Cu_2O:11. For photoelectrochemical water purification, as shown in Figure S3, a three-electrode cell system containing reference (Ag/AgCl), counter (Pt mesh), and working (Cu_2O sample) electrodes was used, which were controlled using a Versastat 3 potentiostat. Furthermore, as the light source for 1 sunlight illumination, a 150 W xenon lamp calibrated with an AM 1.5G filter was used. Figure 5c shows the dependence of the absorbance of the MO peak at 465 nm on the irradiation time. MO stock solutions were prepared in water. In each 15 mL of the MO solution batch, Cu_2O:11 was added under a sunlight source at 0 V_{RHE}, and different batches were removed at an interval of 15 min with a gradual decrease in color intensity, indicating the degradation of the dye (Figure S3). This was also confirmed using UV−visible spectroscopy, as shown in Figure 5d. When Cu_2O:11 with illumination condition photocathode was used, the 465 nm peak decreased more rapidly than that in the dark condition Cu_2O:11 (Figure S4). PEC water purification using a light absorption layer enables energy savings and faster chemical redox reactions than EC or PC water purification.

4. CONCLUSIONS

We developed a method for electrochemically depositing Cu_2O with fine control over its growth direction, resulting in preferred growth along the (111) and (200) crystallographic planes. This selective growth approach enabled the fabrication of Cu_2O-based photoanodes with enhanced efficiency. It has been shown that insignificant adjustments to the initial nucleation and OH^- ion supply significantly impact several material characteristics of Cu_2O, including the crystal orientation, phase, transparency, optical band gap, and electrochemical flat-band potential. First, the mature form of Cu_2O:11 exhibited remarkable capabilities in terms of ultrafast charge transport and transfer. These properties enable significant energy savings and facilitate high-speed independent MO for water purification. This study revealed a positive correlation between enhanced PEC water purification and alterations in photovoltage, which may be attributed to an increase in carrier density. The findings of this study confirm that precise adjustment throughout the electrochemical development process is important to obtain photovoltaic systems based on Cu_2O that exhibit high levels of efficiency. It is posited that the most favorable configuration entails a Cu_2O material showing the (111) orientation in the preferential growth direction, together with the (200) surface facet, in the context of MO water purification. This technological approach is expected to address the pressing issue of rapidly increasing water pollution, offering advantages such as reduced energy consumption and enhanced processing efficiency.

■ ASSOCIATED CONTENT

Supporting Information

The Supporting Information is available free of charge at https://pubs.acs.org/doi/10.1021/acsomega.4c03234.

Pourbaix diagram of Cu-based oxides, optical images of Cu-based oxides, three-electrode cell system for photoelectrochemical water purification, and light absorption data of contaminated water after electrochemical purification (PDF)

■ AUTHOR INFORMATION

Corresponding Authors

Hyung Koun Cho − *School of Advanced Materials Science and Engineering, Sungkyunkwan University, Suwon-si, Gyeonggi-do 16419, Republic of Korea;* orcid.org/0000-0003-0861-523X; Email: chohk@skku.edu

Sung Woon Cho − *Department of Advanced Components and Materials Engineering, Sunchon National University, Suncheon, Jeonnam 57922, Republic of Korea;* orcid.org/0000-0001-8392-3668; Email: swcho@scnu.ac.kr

https://doi.org/10.1021/acsomega.4c03234
ACS Omega 2024, 9, 29723−29731

Authors

Dhruv Sharma − *Department of Advanced Components and Materials Engineering, Sunchon National University, Suncheon, Jeonnam 57922, Republic of Korea*

Dong Su Kim − *School of Advanced Materials Science and Engineering, Sungkyunkwan University, Suwon-si, Gyeonggi-do 16419, Republic of Korea*

Shin Young Oh − *School of Advanced Materials Science and Engineering, Sungkyunkwan University, Suwon-si, Gyeonggi-do 16419, Republic of Korea*

Kun Woong Lee − *School of Advanced Materials Science and Engineering, Sungkyunkwan University, Suwon-si, Gyeonggi-do 16419, Republic of Korea*

Won Seok Yang − *School of Advanced Materials Science and Engineering, Sungkyunkwan University, Suwon-si, Gyeonggi-do 16419, Republic of Korea*

Xuan Zhang − *Department of Advanced Components and Materials Engineering, Sunchon National University, Suncheon, Jeonnam 57922, Republic of Korea*

Sanjay Kumar Swami − *Department of Advanced Components and Materials Engineering, Sunchon National University, Suncheon, Jeonnam 57922, Republic of Korea; Department of Physics, School of Engineering, Dayananda Sagar University, Bengaluru, Karnataka 562112, India;* orcid.org/0000-0002-9156-8317

Complete contact information is available at: https://pubs.acs.org/10.1021/acsomega.4c03234

Author Contributions

‖D.S. and D.S.K. equally contributed to this work. The manuscript was written through contributions of all authors. All authors have given approval to the final version of the manuscript.

Notes

The authors declare no competing financial interest.

■ ACKNOWLEDGMENTS

This research was supported by the National Research Foundation of Korea (NRF) grant funded by the Korean government (NRF-2021R1I1A3060459). This research was also supported by "Regional Innovation Strategy (RIS)" through the National Research Foundation of Korea (NRF) funded by the Ministry of Education (MOE) (NRF-2021RIS-002).

■ REFERENCES

(1) Andreozzi, R.; Caprio, V.; Insola, A.; Marotta, R. Advanced Oxidation Processes (AOP) for Water Purification and Recovery. *Catal. Today* **1999**, *53* (1), 51−59.

(2) Singh, N. B.; Nagpal, G.; Agrawal, S.; Rachna. Water Purification by Using Adsorbents: A Review. *Environ. Technol. Innovation* **2018**, *11*, 187−240.

(3) Mills, A.; Davies, R. H.; Worsley, D. Water Purification by Semiconductor Photocatalysis. *Chem. Soc. Rev.* **1993**, *22* (6), 417−425.

(4) Sun, B.; Li, Q.; Zheng, M.; Su, G.; Lin, S.; Wu, M.; Li, C.; Wang, Q.; Tao, Y.; Dai, L.; Qin, Y.; Meng, B. Recent Advances in the Removal of Persistent Organic Pollutants (POPs) Using Multifunctional Materials: A Review. *Environ. Pollut.* **2020**, *265*, No. 114908.

(5) Westerhoff, P.; Yoon, Y.; Snyder, S.; Wert, E. Fate of Endocrine-Disruptor, Pharmaceutical, and Personal Care Product Chemicals during Simulated Drinking Water Treatment Processes. *Environ. Sci. Technol.* **2005**, *39* (17), 6649−6663.

(6) Sun, J.; Ji, X.; Zhang, R.; Huang, Y.; Liang, Y.; Du, J.; Xie, X.; Li, A. Endocrine Disrupting Compounds Reduction and Water Quality Improvement in Reclaimed Municipal Wastewater: A Field-Scale Study along Jialu River in North China. *Chemosphere* **2016**, *157*, 232−240.

(7) Lingamdinne, L. P.; Koduru, J. R.; Karri, R. R. A Comprehensive Review of Applications of Magnetic Graphene Oxide Based Nanocomposites for Sustainable Water Purification. *J. Environ. Manage.* **2019**, *231* (July 2018), 622−634, DOI: 10.1016/j.jenvman.2018.10.063.

(8) Ajith, M. P.; Rajamani, P. Nanotechnology for Water Purification − Current Trends and Challenges. *J. Nanotechnol. Nanomater.* **2021**, *2* (2), 88−91, DOI: 10.33696/Nanotechnol.2.025.

(9) Kim, D. S.; Lee, K. W.; Choi, J. H.; Lee, H. H.; Suh, H. W.; Lee, H. S.; Cho, H. K. A Durable VO_2 Transition Layer and Defect Inactivation in $BiVO_4$ via Spontaneous Valence-Charge Control. *J. Mater. Chem. A* **2022**, *10* (40), 21300−21314.

(10) Bolisetty, S.; Peydayesh, M.; Mezzenga, R. Sustainable Technologies for Water Purification from Heavy Metals: Review and Analysis. *Chem. Soc. Rev.* **2019**, *48* (2), 463−487.

(11) Savage, N.; Diallo, M. S. Nanomaterials and Water Purification: Opportunities and Challenges. *J. Nanopart. Res.* **2005**, *7* (4−5), 331−342.

(12) Shannon, M. A.; Bohn, P. W.; Elimelech, M.; Georgiadis, J. G.; Marīas, B. J.; Mayes, A. M. Science and Technology for Water Purification in the Coming Decades. *Nature* **2008**, *452* (7185), 301−310.

(13) Duff, W. S.; Hodgson, D. A. A Simple High Efficiency Solar Water Purification System. *Sol. Energy* **2005**, *79* (1), 25−32.

(14) Gonzalez, A.; Grágeda, M.; Ushak, S. Assessment of Pilot-Scale Water Purification Module with Electrodialysis Technology and Solar Energy. *Appl. Energy* **2017**, *206* (October), 1643−1652.

(15) Xie, Z.; Peng, Y. P.; Yu, L.; Xing, C.; Qiu, M.; Hu, J.; Zhang, H. Solar-Inspired Water Purification Based on Emerging 2D Materials: Status and Challenges. *Sol. RRL* **2020**, *4* (3), No. 1900400, DOI: 10.1002/solr.201900400.

(16) Waldner, G.; Brüger, A.; Gaikwad, N. S.; Neumann-Spallart, M. WO_3 Thin Films for Photoelectrochemical Purification of Water. *Chemosphere* **2007**, *67* (4), 779−784.

(17) Ochiai, T.; Fujishima, A. Photoelectrochemical Properties of TiO_2 Photocatalyst and Its Applications for Environmental Purification. *J. Photochem. Photobiol., C* **2012**, *13* (4), 247−262.

(18) Lian, Z.; Tao, Y.; Liu, Y.; Zhang, Y.; Zhu, Q.; Li, G.; Li, H. Efficient Self-Driving Photoelectrocatalytic Reactor for Synergistic Water Purification and H_2 Evolution. *ACS Appl. Mater. Interfaces* **2020**, *12* (40), 44731−44742.

(19) Li, H.; Lyu, J.; Chen, Y.; Jian, L.; Li, R.; Liu, X.; Dong, X.; Ma, C.; Ma, H. Consecutive Metal Oxides with Self-Supported Nanoarchitecture Achieves Highly Stable and Enhanced Photoelectrocatalytic Oxidation for Water Purification. *J. Solid State Electrochem.* **2021**, *25* (3), 1083−1092.

(20) Lin, Y.; Yuan, G.; Liu, R.; Zhou, S.; Sheehan, S. W.; Wang, D. Semiconductor Nanostructure-Based Photoelectrochemical Water Splitting: A Brief Review. *Chem. Phys. Lett.* **2011**, *507* (4−6), 209−215.

(21) Wu, H.; Tan, H. L.; Toe, C. Y.; Scott, J.; Wang, L.; Amal, R.; Ng, Y. H. Photocatalytic and Photoelectrochemical Systems: Similarities and Differences. *Adv. Mater.* **2020**, *32* (18), No. 1904717, DOI: 10.1002/adma.201904717.

(22) Joy, J.; Mathew, J.; George, S. C. Nanomaterials for Photoelectrochemical Water Splitting − Review. *Int. J. Hydrogen Energy* **2018**, *43* (10), 4804−4817.

(23) Hamrouni, R.; Segmane, N. E. H.; Abdelkader, D.; Amara, A.; Drici, A.; Bououdina, M.; Akkari, F. C.; Khemiri, N.; Bechiri, L.; Kanzari, M.; Bernède, J. C. Linear and Non Linear Optical Properties of Sb_2Se_3 Thin Films Elaborated from Nano-Crystalline Mechanically Alloyed Powder. *Appl. Phys. A: Mater. Sci. Process.* **2018**, *124* (12), 861 DOI: 10.1007/s00339-018-2274-1.

(24) Chao, J.; Xie, Z.; Duan, X.; Dong, Y.; Wang, Z.; Xu, J.; Liang, B.; Shan, B.; Ye, J.; Chen, D.; Shen, G. Visible-Light-Driven Photocatalytic and Photoelectrochemical Properties of Porous SnS_x(x = 1,2) Architectures. *CrystEngComm* **2012**, *14* (9), 3163−3168.
(25) Kato, K.; Shirai, T. Highly Efficient Water Purification by WO_3-Based Homo/Heterojunction Photocatalyst under Visible Light. *J. Alloys Compd.* **2022**, *901*, No. 163434.
(26) Wang, R.; Wu, Z.; Chen, X.; Cheng, B.; Ou, W. Water Purification Using a $BiVO_4$/Graphene Oxide Multifunctional Hydrogel Based on Interfacial Adsorption-Enrichment and Photocatalytic Antibacterial Activity. *Ceram. Int.* **2023**, *49* (6), 9657−9671.
(27) Han, S.; Yang, J.; Li, X.; Li, W.; Zhang, X.; Koratkar, N.; Yu, Z. Z. Flame Synthesis of Superhydrophilic Carbon Nanotubes/Ni Foam Decorated with Fe_2O_3 Nanoparticles for Water Purification via Solar Steam Generation. *ACS Appl. Mater. Interfaces* **2020**, *12* (11), 13229−13238.
(28) Wu, T.; Zheng, H.; Kou, Y.; Jin, S.; Jiang, Y.; Gao, M.; Chen, L.; Kadasala, N. R.; Liu, Y. Rhombic Dodecahedral Cu_2O/Ag-3D Fe_3O_4 Micro-Flower Composites for Water Purification under Visible Light Irradiation. *J. Alloys Compd.* **2021**, *858*, No. 157698, DOI: 10.1016/j.jallcom.2020.157698.
(29) Li, H.; Su, Z.; Hu, S.; Yan, Y. Free-Standing and Flexible Cu/Cu_2O/CuO Heterojunction Net: A Novel Material as Cost-Effective and Easily Recycled Visible-Light Photocatalyst. *Appl. Catal., B* **2017**, *207*, 134−142.
(30) Zhan, B.; Liu, Y.; Li, S. Y.; Kaya, C.; Stegmaier, T.; Aliabadi, M.; Han, Z. W.; Ren, L. Q. Fabrication of Superwetting Cu@Cu_2O Cubic Film for Oil/Water Emulsion Separation and Photocatalytic Degradation. *Appl. Surf. Sci.* **2019**, *496*, No. 143580, DOI: 10.1016/j.apsusc.2019.143580.
(31) Kim, D. S.; Kim, Y. B.; Choi, J. H.; Suh, H. W.; Lee, H. H.; Lee, K. W.; Jung, S. H.; Kim, J. J.; Deshpande, N. G.; Cho, H. K. Toward Simultaneous Achievement of Outstanding Durability and Photoelectrochemical Reaction in Cu_2O Photocathodes via Electrochemically Designed Resistive Switching. *Adv. Energy Mater.* **2021**, *11* (39), No. 2101905, DOI: 10.1002/aenm.202101905.
(32) Liu, Y.; Yu, H.; Cui, X.; Gong, Y.; Lu, Y.; Qin, W.; Huo, M. Synthesis of N-$_3N_4$/Cu/Cu_2O: New Strategy to Tackle the Problem of Cu_2O Photocorrosion with the Help of Band Engineering. *Sep. Purif. Technol.* **2022**, *282* (PB), No. 119871.
(33) Das, C.; Ananthoju, B.; Dhara, A. K.; Aslam, M.; Sarkar, S. K.; Balasubramaniam, K. R. Electron-Selective TiO_2 /CVD-Graphene Layers for Photocorrosion Inhibition in Cu_2O Photocathodes. *Adv. Mater. Interfaces* **2017**, *4* (17), No. 1700271, DOI: 10.1002/admi.201700271.
(34) Sun, L.; Lv, G.; Li, W.; Zhang, M.; Feng, H.; Ma, C.; Chen, S. Creating Dual Charge Transfer Channels to Collaborative Enhance the Photocatalytic Bacteriostatic Efficiency and Photocorrosion Resistance of Cu_2O Based Nanocomposites. *Ceram. Int.* **2022**, *48* (11), 15551−15564.
(35) Choi, K. S. Shape Effect and Shape Control of Polycrystalline Semiconductor Electrodes for Use in Photoelectrochemical Cells. *J. Phys. Chem. Lett.* **2010**, *1* (15), 2244−2250.
(36) Amanulla, A. M.; Magdalane, C. M.; Saranya, S.; Sundaram, R.; Kaviyarasu, K. Selectivity, Stability and Reproducibility Effect of CeM - CeO_2 Modified PIGE Electrode for Photoelectrochemical Behaviour of Energy Application. *Surf. Interfaces* **2021**, *22*, No. 100835.
(37) Tiwari, J. N.; Singh, A. N.; Sultan, S.; Kim, K. S. Recent Advancement of P- and d-Block Elements, Single Atoms, and Graphene-Based Photoelectrochemical Electrodes for Water Splitting. *Adv. Energy Mater.* **2020**, *10* (24), No. 2000280, DOI: 10.1002/aenm.202000280.
(38) Kim, D. S.; Oh, S. Y.; Lee, H. H.; Cho, H. K. Harmonized Physical and Electrochemical Process Design for Densely Dispersed Cu Catalysts on Cu_2O Absorbers for Efficient Photoelectrochemical CO_2 Reduction Reaction. *Adv. Energy Mater.* **2024**, No. 2304239, DOI: 10.1002/aenm.202304239.

https://doi.org/10.1021/acsomega.4c03234
ACS Omega 2024, 9, 29723−29731